JACS
JOURNAL OF THE AMERICAN CHEMICAL SOCIETY
Article
pubs.acs.org/JACS

Strong Effects of Cluster Size and Air Exposure on Oxygen Reduction and Carbon Oxidation Electrocatalysis by Size-Selected Pt_n ($n \leq 11$) on Glassy Carbon Electrodes

Sebastian Proch, Mark Wirth, Henry S. White, and Scott L. Anderson*

Department of Chemistry, University of Utah, 315 South 1400 East, Salt Lake City, Utah 84112, United States

Supporting Information

ABSTRACT: Model Pt_n/glassy carbon electrodes (Pt_n/GCE) were prepared by deposition of mass-selected Pt_n^+ ($n \leq 11$) on GCE substrates in ultrahigh vacuum. Electrocatalysis under conditions appropriate for the oxygen reduction reaction (ORR) was studied, for samples both *in situ* with no exposure to laboratory air and with air exposure prior to electrochemical measurements. Of the small clusters, only a few cluster sizes show the expected ORR activity, and in those cases, the activity per Pt atom is similar to that seen under identical conditions with a conventionally prepared electrode with Pt nanoparticles grown on a GCE. For other small Pt_n on GCE, any ORR signal is overwhelmed by large oxidative currents attributed to catalysis of carbon oxidation by water. If the samples are exposed to air prior to electrochemistry, both ORR and carbon oxidation signals are absent, and instead only small capacitive currents or currents attributed to redox chemistry of adventitious organic adsorbates are observed, indicating that air exposure results in passivation of the small Pt clusters.

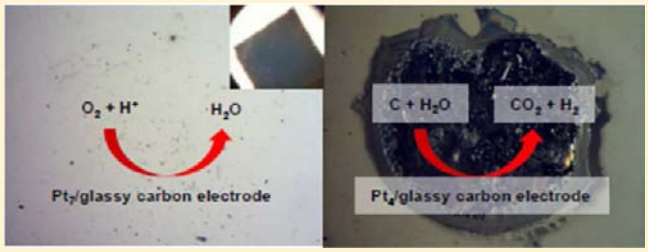

INTRODUCTION

Cell voltage losses in proton exchange membrane fuel cells (PEMFCs) can be grouped into three terms. The first term is the cathode activation overpotential caused by the sluggish oxygen-reduction kinetics. The second describes ohmic losses due to contact resistances between flow fields and the diffusion media as well as due to proton conduction through the membrane. The final term includes the mass transport losses generated mainly by poor oxygen transport through the diffusion medium and the electrode layer. By far the largest losses can be attributed to the cathode activation overpotential.[1] Lowering the cathode overpotential can only be addressed by developing better oxygen reduction reaction (ORR) catalysts (currently Pt and Pt-alloy nanoparticles on various carbon supports).[2] Since the Pt metal content required in the electrodes is also a major practical challenge, an important goal is the design of cheap and stable fuel cell catalysts for the ORR electrode.[3] An obvious approach is to create larger active surfaces at lower precious metal content, i.e., smaller particles.[4] However, various results suggest that the mass activity of Pt clusters has a maximum at around 2 nm particle diameter or a specific surface area of 80 $m^2\ g^{-1}$ of Pt.[2,5,6] A recent investigation by Nesselberger et al.[7] on industrial Pt/C catalysts with an improved experimental design shows increasing mass activity when going from 5 to 1 nm particles. Also a tremendous gain in mass activity was found for Pt_{60}, Pt_{28}, and Pt_{12} synthesized via a dendrimer template.[8] As pointed out by Kunz et al.[9] and Hartl et al.[10] size-selected clusters deposited via the gas phase on a planar substrate are very well-defined model systems for ORR experiments, and measurements for Pt_{20} and Pt_{46} were reported.[9,10] The main advantages of gas-phase deposition are the direct contact between the cluster and the electrode substrate (i.e., no template layer or capping ligands), the reachability of size ranges (Pt_1–Pt_{10}) so far inaccessible by chemical means, and truly monodisperse clusters, at least as they are deposited.

For the present study, size-selected Pt clusters (Pt_n, n = 1–11) were deposited in ultrahigh vacuum (UHV) on glassy carbon electrodes (GCEs) and studied both *in situ* and *ex situ* after exposure to laboratory air. Glassy carbon was chosen because it is a commonly used electrode substrate for ORR studies and is relatively inert under typical operating conditions.[7−12] The surface consists of sp^2-hybridized carbon but does not have a well ordered structure.[13−15] Our primary interests in this study are a comparison of the effects of different cluster sizes and the effects of air exposure on cluster activity, rather than detailed characterization of the electrodes. For this reason we were careful to do all experiments under identical conditions, with (except where noted) identical procedures used to prepare the electrodes. As controls, electrochemical studies were also made of the glassy carbon substrate alone, glassy carbon with nanometer Pt particles prepared by solution deposition, and H_2 annealing and polycrystalline Pt foil electrodes. Dramatic variations in electrochemical behavior with cluster size were observed, and there were also large differences between *in situ* and *ex situ* measurements, with much higher activity observed *in situ*.

Received: October 5, 2012
Published: February 11, 2013

   dx.doi.org/10.1021/ja309868z | *J. Am. Chem. Soc.* 2013, 135, 3073−3086

EXPERIMENTAL METHODS

Clusters are prepared by laser vaporization[16] using an instrument and under conditions that have been described previously.[17−20] The description here focuses on changes made to allow *in situ* electrochemical measurements. The Pt target for laser vaporization was a strip cut from a 99.95% Pt bullion coin, and scraps from the coin were also used to fashion electrodes for bulk Pt control experiments. Cluster cations generated by laser vaporization are collected and transported through five stages of differential pumping by a set of quadrupole ion guides. Midway along the cluster deposition beamline, the ions are mass selected using a quadrupole mass filter with a mass range of ∼4000 amu (Extrel), thereby selecting a particular cluster size. At the end of the beamline, which extends into the UHV deposition/spectroscopy end chamber, clusters are deposited onto a substrate. For these experiments, the substrates were GCEs. The end chamber, shown in Figure S1, is equipped for X-ray photoelectron spectroscopy (XPS) and low-energy He^+ ion scattering (ISS) and also houses gas dosing and mass spectrometry systems not used here as well as an ion gun for sample cleaning. The GCEs were clipped to a tantalum backing plate, which was mounted on the end of a manipulator via a liquid N_2 cryostat and heating wires, allowing temperature control up to ∼1200 K. The end chamber base pressure is $\sim 1 \times 10^{-10}$ Torr.

The UHV system also includes a small antechamber underneath the end chamber, typically used for sample loading and processes requiring high pressures. When the sample is lowered into this antechamber, it is isolated by a differentially pumped triple seal, allowing the antechamber to be pressurized while maintaining UHV in the rest of the system. For these studies, the antechamber was modified to house an electrochemical cell, shown in Figure 1. The cell is mounted on a linear translator, allowing it to be retracted into a side arm of the antechamber when not in use. The cell, constructed of polyether ether ketone (PEEK), consists of a 5 mm diameter, 15 μL working compartment that contains a Pt counter electrode. One end of the working compartment is mated to a reference compartment that communicates with the working compartment via a fritted Vycor plug. The other end of the working compartment is closed by pressing it against an electrode of interest, sealing via a 4 mm diameter O-ring. For these experiments, a Ag/AgCl reference electrode was prepared by dipping a silver wire in hypochlorite solution. Both working and reference sections of the cell are equipped with Teflon tubes used for injecting electrolyte and ports to allow electrolyte solution to flow out of the cell. Electrolyte flows are controlled by a syringe pump located outside the vacuum system.

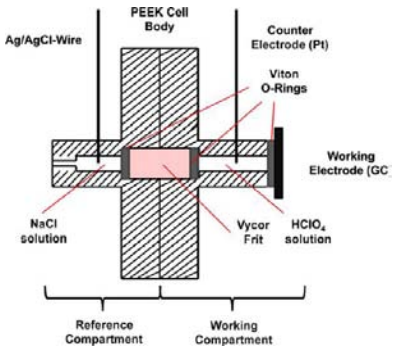

Figure 1. Electrochemical cell for experiments with mass-selected Pt clusters, and cell body made out of PEEK. The cell has two compartments: reference and working. The reference compartment contains an Ag/AgCl electrode in aqueous 3 M NaCl. The working compartment contains a Pt wire counter electrode and is pressed with the Viton O-ring against the glassy carbon working electrode and is filled with 0.1 M aqueous $HClO_4$ solution. The compartments are separated from each other by a Vycor frit (medium) sandwiched between two Viton O-rings to prevent mixing. The compartments also include Teflon tubes for solution inlets and ports for solution outlet. Further information is provided in the Figure S1.

To allow *in situ* electrochemical measurements, an electrode (e.g., a GCE with deposited Pt_n) is first prepared in the UHV end chamber, as described below, and then lowered through the triple seal into the center of the antechamber while the electrochemical cell is retracted. The antechamber was vented to ∼1 atm with high-purity argon, and then the linear translator holding the electrochemical cell was used to push the electrochemical cell against the surface of the GCE, sealing via the O-ring at the open end of the working section. To achieve sufficient sealing force, the sample is supported from the back side, by pushing a Teflon rod against the tantalum backing plate using a linear motion feedthrough. Finally, the working and reference sections of the cell are filled with electrolyte, and electrochemical studies are carried out.

As shown below, exposure of the samples to air can dramatically affect activity, thus for the *in situ* work we minimize exposure to adventitious adsorbates. Prior to each experimental cycle, the antechamber is baked to 400 K overnight while being pumped by a turbomolecular pump, then allowed to cool while the electrode is being prepared in the UHV end chamber. From the time the sample is lowered into the antechamber until the antechamber is vented with argon, the sample is exposed to a base pressure of $\lesssim 3 \times 10^{-8}$ Torr for a few minutes. The base pressure of the antechamber under normal conditions is $<10^{-9}$ Torr, and the higher pressure in the present experiments reflects the fact that the antechamber still has elevated water vapor pressure remaining from the previous day's electrochemical work, which saturates the chamber with water vapor. Because the samples are wetted with aqueous electrolyte as soon as the cell is sealed, we do not expect that prior exposure to a few Langmuirs of water vapor (1 L = 10^{-6} Torr·sec) during transfer/sealing should have a significant effect.

In addition to electrochemical measurements, the antechamber was used as a load lock, to remove GCEs for *ex situ* studies, to introduce fresh GCEs for each deposition experiment, and to introduce electrodes prepared *ex situ* for control studies with the *in situ* cell. *Ex situ* work included electrochemistry done in a benchtop cell, electrode analysis by XPS (Kratos Axis Ultra), and optical and scanning electron microscopy (SEM−FEI NovaNano).

The GCEs were prepared by dicing 1 mm thick glassy carbon sheets (CH Instruments, ALS Ltd., Tokyo) into 6 × 6 mm squares. We initially experimented with polishing the GCEs using alumina powder (1 μm, then 0.3 μm, then 0.05 μm), however, atomic force microscopy examination (see Figure S2) showed that polishing simply made the surfaces rougher, therefore experiments were performed with as-received electrodes, with ∼2 nm roughness. Before each deposition experiment, a fresh GCE sample was mounted to the manipulator in the antechamber. After evacuating the antechamber with a turbomolecular pump overnight while heating the antechamber to 400 K, the CGE was raised into the UHV end chamber and heated to 900 K in UHV for 60 min to degas adventitious adsorbates, detectable as O 1s signal in XPS. After the 900 K degassing, XPS shows nothing but carbon on the GCEs, as shown in Figure S3.

The experimental protocol for the size-selected cluster experiments was as follows: For all experiments, Pt_n^+ were mass selected and deposited at a nominal energy of ∼1 eV/atom on a fresh, degassed, room temperature GCE. Pt coverage was determined by integrating the deposition current, and deposition was terminated when the desired coverage was reached. The 2 mm diameter cluster spot size was controlled by a deposition mask and was checked by profiling using XPS. In each experiment, the 2 mm spot received a total of 4.5×10^{12} Pt atoms in the form of a particular Pt_n, corresponding to ∼9.5% of the Pt density in a close-packed Pt(111) surface (i.e., ∼0.1 ML equivalent). After Pt_n^+ deposition, the electrodes were again characterized by XPS. Some samples were also characterized by ISS, however, those samples were not used in electrochemistry experiments, to avoid artifacts due to He^+ impact damage. After XPS characterization of the as-deposited electrodes, the electrodes were inserted into the antechamber for either *in situ* electrochemistry or

extraction for *ex situ* electrochemistry on the benchtop under atmospheric conditions.

A potential problem is that sintering of deposited Pt_n might tend to destroy any size-dependent properties we seek to observe. Because of the rather rough glassy carbon surface, none of the available experimental methods (ISS, SEM, XPS) provide any direct evidence on this issue nor would STM or AFM, if available, be likely to be able to image such small clusters on a rough surface. As we will show below, however, the Pt_n/GCE samples show strong, sharp, and nonmonotonic dependence on deposited cluster size of both the electrochemical activity and the Pt 4f binding energies. These observations rule out substantial sintering, at least for clusters with more than ~6 atoms.

In a few preliminary experiments, the samples were reanalyzed *in situ* after electrochemical measurements, by flushing the electrochemical cell with water, followed by ethanol, and then drying the samples in the antechamber before pulling them back into the end chamber for XPS and/or ISS analysis. These samples showed significant reduction in Pt signal, however, they also showed significant Cl signal, indicating that some electrolyte remained adsorbed. For this reason, it is essentially impossible to interpret the Pt intensity loss, and therefore we discontinued this analysis step.

For *in situ* electrochemistry experiments, the antechamber is filled to ~1 atm with high purity argon, and then the electrochemical cell is sealed to the GCE, surrounding the cluster-containing spot. The area of the GCE exposed to the electrolyte solution is defined by the O-ring seal. The reference compartment of the cell is then filled with 3 M aqueous NaCl solution, and the working compartment is filled with either nitrogen- or oxygen-saturated 0.1 M aqueous $HClO_4$ electrolyte. All electrochemical solutions are prepared from 18 MΩcm water (Barnstead E-pure filter system) and high purity grade chemicals. Gas saturation in the working electrolyte is achieved by bubbling nitrogen or oxygen through the solution for at least 20 min prior to the experiment. Cyclic voltammograms (CVs) were acquired using a CH Instruments model 600D potentiostat. Because the CVs exhibited considerable noise when electrolyte was flowing through the cell, they were taken under static conditions, however, the cell was flushed with fresh electrolytes between each set of CVs.

Data acquisition for the *in situ* experiments always took place in the form of a sequence of CVs over increasing voltage ranges, designed with two goals in mind. We were concerned that our very small Pt clusters might dissolve or otherwise be irreversibly changed if the potential was scanned through ranges where Pt oxidation occurs (>0.988 V vs Ag/AgCl for bulk Pt). Therefore, the initial CVs focused on the potential range where ORR is expected. Potentials above 0.4 V were avoided, based on the possibility that oxidation of small Pt clusters might occur at lower potentials than for bulk Pt. In addition, we never scanned into ranges where water electrolysis might generate gas bubbles, leading to current blockage in our very small cell. In the CV sequence listed below, all potentials are given relative to Ag/AgCl, and all CVs were initially scanned from a positive starting potential to −0.1 V and then back to the starting potential. The following protocol was employed except where noted in the text:

(1) A single CV cycle was recorded between 0.2 and −0.1 V in N_2-saturated 0.1 M $HClO_4$.
(2) The initial potential was increased to 0.4 V, and a single CV cycle was recorded between 0.4 and −0.1 V in N_2-saturated 0.1 M $HClO_4$.
(3) 10−100 CV cycles were recorded between 0.4 to −0.1 V in N_2-saturated 0.1 M $HClO_4$.
(4) The solution was replaced with an O_2-saturated 0.1 M $HClO_4$ solution, and steps (1−3) were repeated to examine ORR activity.
(5) The initial potential was increased to 1.3 V and one CV was recorded between 1.3 and −0.1 V in O_2-saturated solution.
(6) 100 CV scans were recorded between 1.3 V and −0.1 V in the O_2-saturated solutions.
(7) The solution was then replaced by the N_2-saturated solution, and a CV scan was recorded between 1.3 and −0.1 V.
(8) 100 CV scans were recorded between 1.3 V and −0.1 V in N_2-saturated solution.

Comparison of experiments (1−4), where V_{max} never was allowed to go into the range where Pt oxidation might occur, allows us to examine the ORR efficiency for the different clusters. The wider potential range scans, steps (5−8), allow us to examine Pt oxidation and changes in the currents that result from repeated oxidation/reduction of the Pt.

Some experiments described below resulted in gas evolution in the working section of the cell, which typically formed bubbles that blocked the current in the small diameter cell. The scan rate for all Pt_n/CGE CVs was initially set at 0.1 V s^{-1}, however, when current blockage by bubbles was observed, the scan rate was increased to 1 V s^{-1} to minimize interference from bubbles. We were unable to achieve fast enough electrolyte flows to flush the bubbles from the cell via the normal electrolyte outflow ports, therefore when bubble blockage occurred, it was necessary to break the seal of the cell to the GCE surface (in the clean argon atmosphere), allowing bubbles to be flushed out the open end of the cell, prior to resealing the cell to the GCE. A metal cup was positioned under the cell to catch the electrolyte flushed from the cell. After completion of the electrochemical experiments, the antechamber was opened, the electrode was extracted for postreaction analysis, and spilled electrolyte was washed out prior to mounting a fresh GCE to the end of the manipulator. The antechamber was then evacuated to the low 10^{-8} Torr range overnight while baking at 400 K to degas the antechamber and GCE sample, prior to moving the sample into the UHV chamber for 900 K degassing and cluster deposition.

The effects of exposure to laboratory air on the deposited cluster electrodes were probed by preparing Pt_n/GCE samples in UHV, as for the *in situ* study, but then removing them for study in air. For these experiments, the entire antechamber, with electrochemical cell, was removed from the vacuum system and set up on the benchtop, so as to maintain identical geometry and conditions to those used in the *in situ* work, apart from air exposure. For those experiments, a second antechamber was used as a load lock for sample exchange.

Several sets of reference experiments were performed. Polycrystalline Pt foil ("Pt_{poly}") was studied both *in situ* and *ex situ*. For *ex situ* experiments, Pt_{poly} was cleaned in aqua regia and then further cleaned by repeated CV cycling in $HClO_4$ electrolyte (Figure S4). As shown by XPS in Figure S5, the aqua regia-cleaned Pt_{poly} is oxidized and has adventitious carbon contamination, which is removed in the CV cycling. For *in situ* experiments with Pt_{poly}, the Pt foil was sputtered and annealed in UHV, and this electrode was shown by XPS to be metallic Pt with negligible carbon contamination (Figure S5).

Experiments were also performed both *in situ* and *ex situ* using GCEs covered with Pt nanoparticles grown by solution deposition and H_2 reduction ("Pt_{nano}"). Pt_{nano} electrodes were prepared by dissolving hexachloroplatinic acid (H_2PtCl_6) in absolute ethanol. The GCE was sonicated for 20 min in absolute ethanol for cleaning, and then the hexachloroplatinic acid solution was drop coated onto the GCE. The modified GCE was dried in air and then heated to 473 K in a hydrogen stream for 120 min, resulting in reduction to elemental Pt and aggregation to form Pt nanoparticles on the GCE. Ethanol was used for Pt_{poly} deposition because initial attempts using hexachloroplatinic acid in water resulted in substantial silicon contamination of the electrode surfaces, as seen by XPS, even when using 18 MΩcm water and Teflon containers for solution handling. XPS of Pt_{nano} electrodes prepared from ethanol solution showed only carbon and Pt.

We certainly do not claim that our *in situ* procedure results in no exposure to adventitious adsorbates (impossible even in UHV experiments!); however, several observations reported below suggest that the effects of such adsorbates are minimal: (1) Electrodes prepared and studied *in situ* are vastly more active than identical electrodes deliberately exposed to air prior to electrochemical study. (2) The CVs for both Pt_{nano} and Pt_{poly} cleaned by UHV techniques and studied using the same *in situ* techniques as the Pt_n/GCE samples show structure similar to CVs obtained for the same electrodes cleaned by electrochemical means, consistent with literature CVs for such

dx.doi.org/10.1021/ja309868z | J. Am. Chem. Soc. 2013, 135, 3073−3086

samples after electrochemical cleaning. (3) For a glassy carbon electrode prepared in UHV, one might expect that significant concentrations of adventitious adsorbates would result in significant redox peaks during *in situ* CV experiments. As shown below, the *in situ* CV peaks for vacuum-cleaned GCEs have amplitudes of only ~1 μA/cm^2, which is negligible on the scale of the signals coming from Pt-containing samples.

RESULTS

Reference Experiments. Before discussing the experiments with size-selected clusters, it is useful to briefly discuss the results of reference experiments, both to verify that the *in situ* electrochemical cell works properly and to provide data using conventional electrodes for comparison to the cluster-containing electrodes. Since these experiments were on systems that have been studied thoroughly by previous researchers, the data and discussion can be found in the Supporting Information (SI), and only a brief summary of the results relevant to interpretation of the size-selected experiments is given here.

Pt_{poly} (Polycrystalline Bulk Platinum). After first verifying that we obtained the expected results[21−23] for an electrochemically cleaned Pt electrode in a benchtop cell (Figure S4), we then confirmed the expected behavior for a polycrystalline Pt electrode using the *in situ* cell and procedures as described above. Because the *in situ* cell is easily blocked by bubbles, it was not possible to use electrochemical cycling over a wide potential range to clean the Pt electrode. Instead, the polycrystalline Pt electrode was cleaned with aqua regia, sonicated in ethanol, then mounted to the manipulator as described for the GCEs, and cleaned by sputtering and annealing in UHV. The procedure for doing *in situ* electrochemistry with this Pt_{poly} electrode was identical to that used for the Pt_n/GCE samples described above. Figure S5 shows XPS of the electrode before and after sputter cleaning and CVs taken *in situ* for both N_2- and O_2-saturated 0.1 M $HClO_4$ aqueous electrolytes. In N_2-saturated $HClO_4$, the expected electrochemical waves associated with reversible Pt oxidation and formation of Pt surface hydrides are observed. In the O_2-saturated electrolyte, a broad wave associated with ORR is also observed.

Glassy Carbon Electrodes (GCE). Because the Pt loading in the size-selected Pt_n experiments is quite low, it is important to establish whether there is any electrochemical activity for the clean Pt-free GCE material under the same conditions used in the Pt_n/GCE work discussed below. The results are shown in Figure 2. The GCE was mounted on the manipulator, baked to 900 K in UHV, then lowered into the antechamber, and mated with the *in situ* electrochemical cell, as described above. The CVs obtained in both N_2- and O_2-saturated aqueous 0.1 M $HClO_4$ are shown. The CVs show a few μA/cm^2 of capacitive current as well as small peaks (~0.5 V vs Ag/AgCl) that are probably associated with oxidation/reduction of surface functional groups or adventitious adsorbates. These redox peaks have amplitudes of only ~1 μA/cm^2, compared to much larger features observed when Pt_n are present, suggesting that the effects of such adsorbates or surface functionalization are small. After subjecting the GCE to ~120 CV cycles over potential ranges up to 1.3 to −0.1 V vs Ag/AgCl and back, there is no visual sign of electrode deterioration nor is any observed by optical microscopy (Figure S6).

GCE with Solution-Deposited Platinum (Pt_{nano}). The final reference experiments were with GCE electrodes containing nanometer-scale Pt particles, prepared by solution deposition of

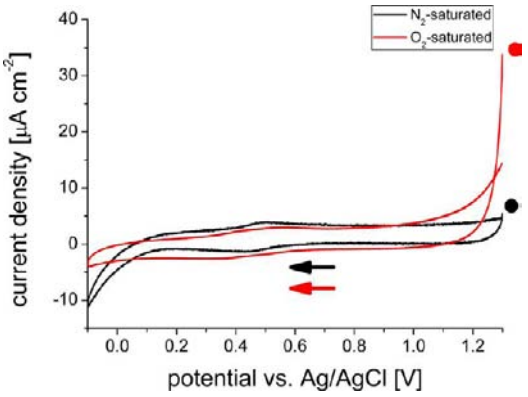

Figure 2. Electrochemistry of a clean GCE *in situ*. CVs of glassy carbon in 0.1 M $HClO_4$ under N_2- and O_2-saturated conditions at a scan rate of 0.1 V s^{-1}. The initial potential of the CV was 1.3 V vs Ag/AgCl.

H_2PtCl_6 and hydrogen reduction. Figure S7 shows XPS and SEM characterization of the Pt_{nano} electrode prior to electrochemical study. The Pt-loading determined by XPS is ~1 ML equivalent of Pt, and the Pt is metallic, with SEM-visible particles mostly in the 10 nm range, with a few larger particles up to ~50 nm. The Pt_{nano}/GCE sample was introduced to the lower antechamber of the vacuum system, evacuated to ~1 × 10^{-6} Torr and mated with the *in situ* electrochemical cell, after venting the antechamber with argon. Figure 3 shows CVs for Pt_{nano} in the *in situ* cell with N_2- and O_2-saturated 0.1 M $HClO_4$. For N_2-saturated electrolyte, PtO_x reduction and hydride adsorption are observed during the sweep to negative potential, and hydride desorption and Pt oxidation features are observed on the return sweep to 1.3 V, although these are not as obvious as in the Pt_{poly} case. In O_2-saturated electrolyte, there is a large reduction wave at potentials below ~0.4 V vs Ag/AgCl, comparable to what is observed with Pt_{poly}. This wave includes overlapping contributions from ORR, PtO_x reduction, and hydride adsorption. On the return sweep to 1.3 V, hydride desorption is buried in the ORR wave, but Pt oxidation is clearly seen above ~0.9 V vs Ag/AgCl. The Pt oxidation/reduction and hydride adsorption/desorption waves are less distinct than for Pt_{poly}, as expected because the fraction of the electrode surface covered with Pt is relatively small. Optical microscopy of the Pt_{nano} electrode after ~150 CV cycles over potential ranges up to 1.3 to −0.1 V vs Ag/AgCl shows no evidence of electrode degradation, as shown in the lower frame of the figure.

***In Situ* Experiments on Size-Selected Pt_n/GCE.** *XPS and ISS Characterization of As-Deposited Pt_n/GCE.* Figure 4 shows the Pt $4f_{7/2}$ binding energies determined by fitting raw XPS data (Figure S8 and discussion in SI) for the as-deposited Pt_n/GCEs. The estimated uncertainty in the binding energies is ~0.1−0.2 eV, resulting primarily from the low Pt concentration in the samples and corresponding low signal/noise in the spectra.

The fact that the binding energies have strong and nonmonotonic dependence on cluster size demonstrates that the samples retain memory of the deposited cluster size. If diffusion and sintering of the deposited Pt were efficient, this would tend to wipe out the effects of size on the binding energy. A general trend of decreasing binding energy with increasing cluster size is expected for reasons discussed below, however, the oscillatory structure indicates size-dependent

dx.doi.org/10.1021/ja309868z | J. Am. Chem. Soc. 2013, 135, 3073−3086

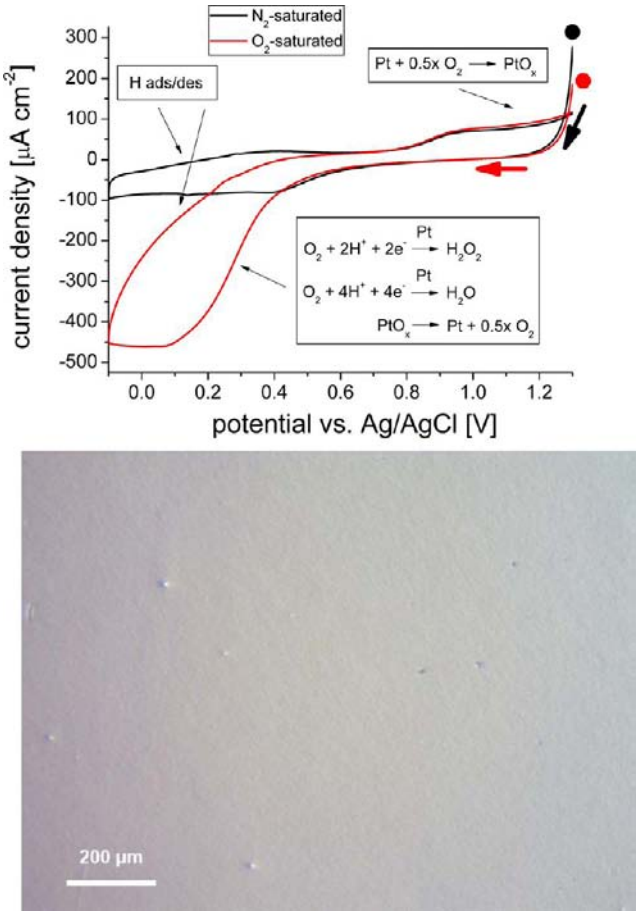

Figure 3. Pt_{nano}/GCE *in situ* (1 ML Pt). (Top) CVs in N_2- and O_2-saturated 0.1 M $HClO_4$ solutions at a sweep rate of 0.1 V s^{-1} The initial potential of the CV was 1.3 V vs Ag/AgCl. The reduction wave is a combination of two- and four-electron oxygen reduction, Pt oxide reduction, and hydride adsorption/desorption. (Bottom) Optical micrograph of the Pt_{nano}/GC electrode after the electrochemical measurements. Shown is a region within the perimeter of the attached electrochemical cell. The entire electrode was covered with nanoparticles in this case.

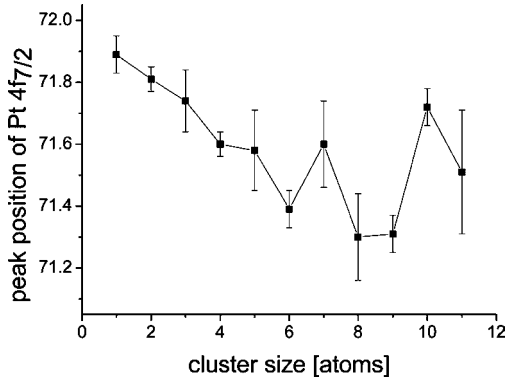

Figure 4. Pt $4f_{7/2}$ peak position for as-deposited Pt_n/GCE (n = 1−11) as a function of the cluster size. Multiple deposition data were collected for all cluster sizes except Pt_{11}. The error bars arise from the standard deviation of the different shifts from different deposition experiments, except for Pt_{11}, where the error bar arises from the fitting procedure with constant separation between Pt $4f_{7/2}$ and Pt $4f_{5/2}$ peaks (3.33 eV) and variable peak widths.

variations in cluster electronic structure. In this case, the binding energies for some of the clusters are already close to that for bulk Pt (71.2 eV).[24] The binding energies observed here for Pt_n/GCE are in the same range as those observed for Pt_n/TiO_2 by Watanabe et al.[25]

The intensities are also interesting. Figure S9 compares the XPS and ISS signals measured *in situ* for samples prepared by deposition of Pt_1 (10% ML) on glassy carbon, with analogous results for the same amount of Pt_1 deposited on rutile TiO_2(110), used as an atomically flat reference substrate, where Pt is known to remain on the surface at room temperature.[26] It can be seen that the Pt XPS intensity on the GCE is about half that observed on TiO_2, which is well outside the typical reproducibility of our deposition coverages (typically within ∼10%, mainly due to variations in the size of the cluster spot relative to the 1.1 mm spot probed by XPS). X-ray penetration lengths in carbon are far too large (∼65 μm)[27] for the ±2 nm surface roughness to cause significant attenuation of X-rays reaching the Pt at the 54.7° angle of incidence, therefore, the ∼50% intensity loss must be attributed to attenuation of electrons emitted by Pt. Given the high electron kinetic energy for Pt 4f XPS, the electron attenuation length is ∼1.2 nm for penetration through Pt and ∼3.3 nm for penetration through carbon.[28] Attenuation could be taken as evidence that the deposited Pt atoms sinter into large particles, which would need to be four to five layers thick to give an average attenuation of 50%, however, the strong and nonmonotonic dependence of the Pt 4f binding energy (and electrochemical results below) on deposited cluster size appears to rule out extensive sintering. Another possibility might be Pt diffusion into pores or other nanostructure in the glassy carbon, and analysis of the CGEs after electrochemical studies (see below) provides some evidence that electrocatalysis may be taking place beneath the GCE surface layer. Although the supplier of our GCE material (ALS Ltd., Tokyo) states that there is 0% porosity, it is not clear whether this excludes small pores that might allow some Pt to diffuse a nanometer or two into the GCE.

As shown in Figure S9, the Pt ISS signal for Pt/GCE is ∼10 times smaller than that for the same amount of Pt on TiO_2, reflecting the fact that ISS largely probes atoms in the topmost layer of the sample. As with XPS, the low ISS signal for Pt/GCE could result from sintering into multilayer Pt particles, although to get 10-fold attenuation, the particles would have to be roughly 10 layers thick, and in that case, the XPS would be attenuated by more than a factor of 2. Pt on the GCE surface could also be shadowed by the ∼2 nm roughness of the GCEs, but only if the roughness is such that most of the deposited Pt is invisible to He^+ incident at 45° with respect to the surface plane. The AFM data (Figure S2) suggest that the surface is not so rough, but tip convolution would prevent the AFM from seeing sharp features or small pores that might shadow subnanometer clusters.

Electrochemistry of Pt_7 on GCEs (in Situ): A "Normal" Cluster. We first present results for Pt_7/GCE, because this cluster size shows behavior most similar to that seen for conventionally prepared Pt electrodes, such as Pt_{nano} and Pt_{poly}. Figure 5A compares CVs obtained in N_2- and O_2-saturated $HClO_4$ between 0.4 and −0.1 V, where Pt oxidation should not be possible (CV experiments (2) and (4) in the sequence given above). Comparison of the scans for O_2- and N_2-saturated $HClO_4$ shows clear evidence of extra structure, and comparison with the data for the Pt_{nano}/GCE reference sample (Figure 3 top) suggests that the feature around 0.2 V results from ORR,

dx.doi.org/10.1021/ja309868z | J. Am. Chem. Soc. 2013, 135, 3073−3086

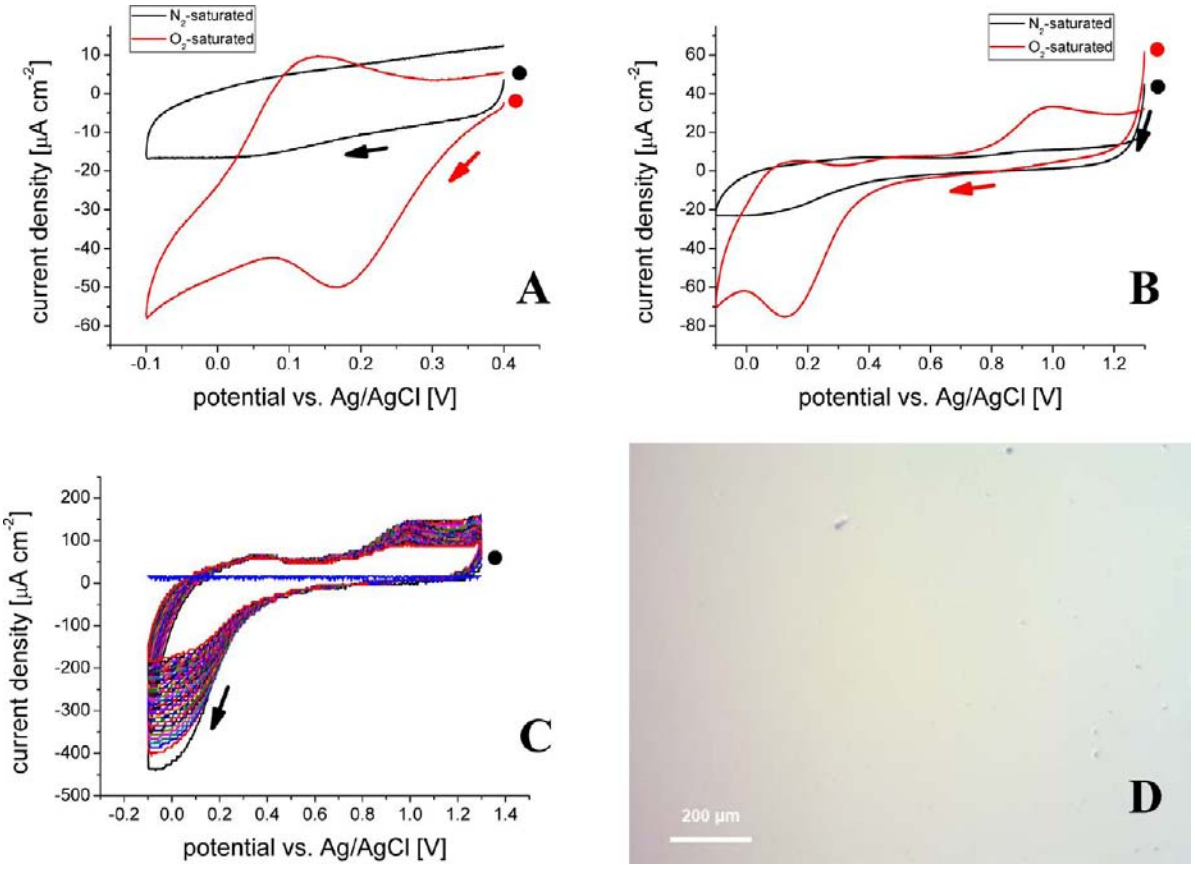

Figure 5. Pt_7/GCE *in situ* (0.1 ML Pt). (A) CVs in N_2- and O_2-saturated 0.1 M $HClO_4$ at a sweep rate of 0.1 V s^{-1} (initial scan from 0.4 to −0.1 V vs Ag/AgCl). (B) CVs in N_2- and O_2-saturated 0.1 M $HClO_4$ at a sweep rate of 0.1 V s^{-1} (initial scan from 1.3 to −0.1 V vs Ag/AgCl). (C) CVs in O_2-saturated 0.1 M $HClO_4$ at a sweep rate of 1 V s^{-1} (initial scan from 1.3 to −0.1 V vs Ag/AgCl, 100 cycles, bubble formation resulted in current loss on the 44th cycle). The colors show the different cycles with black being the first and red the last cycle; the currents on each subsequent CV are decreasing indicating a loss of active Pt surface area. The reduction wave observed in (A−C) is a combination of oxygen reduction, Pt oxide reduction, and hydride adsorption/desorption. (D) Optical micrograph of the Pt_7/GC electrode after the electrochemical experiments.

with currents that are roughly 5 times smaller than those for Pt_{nano}. Note, that the Pt loading is 10 times lower for Pt_7 than for Pt_{nano}, thus the current per Pt atom is roughly double that for larger Pt nanoparticles, presumably because the small clusters have most or all of the Pt atoms in the surface layer and are more dispersed and thus less constrained by O_2 diffusion. This ORR wave may have contributions from both four-electron reduction of O_2 ($O_2 + 4H^+ + 4e^- \rightarrow 2\ H_2O$) and two-electron reduction of O_2 ($O_2 + 2H^+ + 2e^- \rightarrow H_2O_2$). It is unlikely, however, that reduction of oxidized Pt ($PtO_x \rightarrow Pt + 1/2x\ O_2$) contributes significantly, both because this sample had been cycled to potentials close to the range where Pt oxidation would be expected (> ∼0.6 V vs Ag/AgCl for surface Pt) and because no reduction wave was seen for the N_2-saturated case. Compared to the results observed for other cluster sizes shown below, this Pt_7/GCE sample looks "normal" in that it exhibits oxygen reduction behavior, and currents are in the expected range.

The second frame of the figure (Figure 5B) compares CVs run between 1.3 and −0.1 V in N_2- and O_2-saturated 0.1 M $HClO_4$ (scans (5) and (8) in the sequence given above), i.e., starting the scans in the potential range where Pt might be expected to oxidize and cycling through potentials where Pt should be reduced. In the CV for O_2-saturated solution, there are substantial reduction features around 0.15 and −0.1 V vs Ag/AgCl, which we attribute to some combination of O_2 reduction, PtO_x reduction, and adsorption of hydrides. On the return sweep, a wave is observed around 0.1 V vs Ag/AgCl, likely due to hydride desorption, and a larger wave around 1 V vs Ag/AgCl is attributed to Pt oxidation. The integrated amplitude of this feature at ∼1 V is consistent with oxidation of all the Pt atoms in the sample. The lack of expected Pt reduction/oxidation features for the N_2-saturated CV is discussed below.

Figure 5C shows a series of 100 CVs taken in O_2-saturated $HClO_4$, under static conditions, just after completion of the O_2-saturated scan in part B of the figure. The current is largest in the first cycle and decays monotonically during cycling. After 44 cycles, the current suddenly decreased to zero, which we attribute to electrode blockage by bubble formation. The rate of decay of the current during cycling is too large to be explained by depletion of O_2 by ORR. O_2 saturation should lead to ∼1 mM O_2 concentration in the electrolyte or 15 nmol O_2 in the 15 μL cell. The integrated current associated with the irreversible ORR is 4×10^{-6} C per CV cycle, therefore complete depletion of the O_2 would require ∼1000 CV cycles, assuming that the currents remain constant and O_2 does not escape the cell in other ways. The fact that the current decays by 50% in ∼44 CVs suggests that there is an additional deactivation mechanism. The observation that the wave around 1 V, attributed to Pt oxidation, also diminishes suggests that active Pt surface area is being lost, and this Pt loss would also

dx.doi.org/10.1021/ja309868z | J. Am. Chem. Soc. 2013, 135, 3073−3086

decrease ORR activity. Most likely, the Pt loss occurs because the scan range runs above the potential required for Pt oxidation (> ~0.6 V vs Ag/AgCl for surface Pt), and repeated oxidation/reduction cycles are resulting in either Pt dissolution[29] or sintering.

The CV between 1.3 and −0.1 V for N_2-saturated $HClO_4$ (Figure 5B) was taken after the sequence of 100 CVs in O_2-saturated electrolyte shown in Figure 5C. It can be seen that the expected features for Pt oxidation and reduction are greatly attenuated, compared to what should be seen if the active area of Pt were still the same as in the initial CVs [compare, e.g., the Pt oxidation features for Pt_{nano} in O_2- and N_2-saturated $HClO_4$ (Figure 3)]. This weakness of signals expected for Pt in N_2-saturated electrolyte is consistent with the conclusion that Pt surface area was lost during repeated cycling through the Pt oxidation and reduction potentials (Figure 5C).

It is interesting to compare the potentials and currents associated with the ORR feature observed for Pt_7 and the analogous results for conventionally prepared electrodes. The onset of the ORR wave (taken as the potential where the current for O_2- and N_2-saturated cases deviate) is at ~0.8 V vs Ag/AgCl for the Pt_{poly} sample. For the Pt_{nano}/GCE sample, the onset is at 0.4 V and for the Pt_7/GCE sample, ORR starts at about 0.6 V. Quantitative analysis of the current densities obtained per Pt atom is difficult because these experiments were done in a static cell, where influences of diffusion on the limiting currents are expected to be highly sensitive to sample morphology. For Pt_{poly} the surface is approximately planar and entirely Pt. For Pt_{nano}, the surface has ~10 nm Pt particles separated by tens of nanometers on the surface, while for Pt_7/GCE, the clusters are subnanometer with average center-to-center separation of ~2 nm (as deposited). If a potential of 0.3 V vs Ag/AgCl is used for comparison (at this potential all samples show reductive currents and are not yet at the mass-transfer limit), then the current per Pt atom is 2×10^{-19} A/atom for Pt_{poly}, 1.3×10^{-19} A/atom for Pt_{nano}, and 2.7×10^{-19} A/atom for Pt_7. This means that Pt_7 does not lower the overpotential for the ORR but is a highly active catalyst in the high overpotential region for ORR.

The Pt_7/GCE sample was subjected to a total of >200 CV cycles in N_2- and O_2-saturated $HClO_4$ over ranges up to 1.3 to −0.1 V vs Ag/AgCl, prior to being removed from the instrument for postreaction analysis. As shown by the optical micrograph at the bottom of Figure 5, this sample showed no deterioration of the electrode, similar to the lack of deterioration seen for both Pt_{nano}/GCE and Pt-free GCE. To the eye, the electrode appears shiny black, with no obvious difference between the inner region exposed to the $HClO_4$ electrolyte and the outer, unexposed region. The entire sequence of >200 CVs under different conditions was replicated on two different Pt_7/GCE samples, in addition to the *ex situ* measurements performed on a third and fourth sample, discussed below.

Electrochemistry of Pt_4 on GCEs (in Situ): A Typical Small Cluster. In contrast to Pt_7 on GCEs, which has electrochemical behavior similar to conventional Pt electrodes (Pt_{poly}, Pt_{nano}), the samples prepared with Pt_n in the $n = 1-6$ range displayed a very different behavior. Results for samples with Pt_1, Pt_2, Pt_3, Pt_5, Pt_6, Pt_8, and Pt_{10} on GCEs are presented in the Figures S10−S16. Here we present the results for Pt_4/GCE, typical of the clusters with $n \leq 6$. The raw XPS of Pt_4 as deposited on a GCE is shown in Figure S8.

Electrochemical experiments on Pt_4/GCE under conditions identical to those used for Pt_7/GCE are summarized in Figure 6. As shown by the CVs in the top frame of the figure,

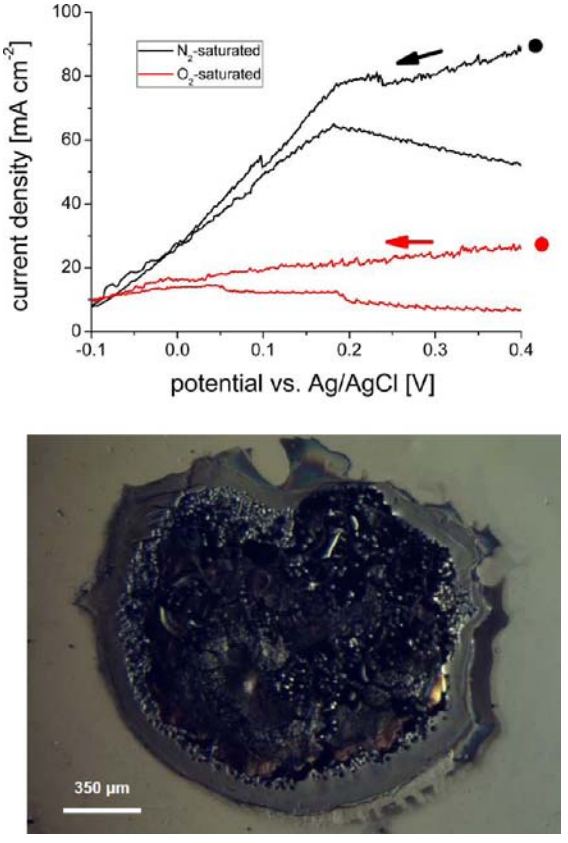

Figure 6. Pt_4/GCE *in situ* (0.1 ML Pt). (Top) CVs of Pt_4/GCE in N_2- and O_2-saturated 0.1 M $HClO_4$ at a scan rate of 1 V s^{-1} (initial scan from 0.4 to −0.1 V vs Ag/AgCl). (Bottom) Optical micrograph of the Pt_4/GC electrode after the electrochemical experiments.

enormous currents were observed, corresponding to oxidation occurring at Pt_4/GCE. The current appears to become limited for E > ~0.2 V vs Ag/AgCl, saturating at currents of tens of mA/cm^2. Note that the scan for the N_2-saturated solution was done first, and the lower currents for the O_2-saturated solution reflect damage to the electrode (see below). The cell currents were somewhat erratic and went irreversibly to zero after a few CV cycles. Note that this CV was obtained at a scan rate of 1 V s^{-1}, compared to the 0.1 V s^{-1} rate used for the previously discussed experiments. We initially attempted CVs for Pt_4/GCE at 0.1 V s^{-1}, however, for such slow scans, not even a single CV could be completed before the current went abruptly and irreversibly to zero.

While we cannot see into the *in situ* cell during operation, the sudden current loss is attributed to blockage of the 15 μL working section of the cell by bubble formation. Such blockages are observed, for example, in any experiment with any type of electrode, whenever the potential is scanned into a range where water electrolysis occurs. When bubble blockage occurs, cell current can be restored by breaking the seal to the electrode surface to allow the bubbles to be flushed out, as discussed in the Experimental Methods section. The interesting point is that water electrolysis should not be possible in the potential range where the huge currents and apparent gas formation are

dx.doi.org/10.1021/ja309868z | J. Am. Chem. Soc. 2013, 135, 3073−3086

observed for Pt_4/GCE, indicating that some other reaction is generating large oxidation currents and copious gas.

To provide insight into the nature of this oxidation reaction, the electrode was removed from the instrument for examination after 20 CV cycles between 1.3 to −0.1 V vs Ag/AgCl, in both N_2- and O_2-saturated $HClO_4$ at 1 V s^{-1} scan rate. During the course of these CVs, it was necessary to break open and flush the cell five times in order to restore the current after bubble blockage. The electrode destruction observed is readily apparent in a micrograph (Figure 6, bottom frame), and the appearance can be described as follows: Before electrochemical measurements, the GCE is black with a mirror finish. Because of the near-specular lighting used, this shiny surface appears light gray in the micrograph, as in the outer regions of the image, which correspond to the area that was outside the cell and therefore unchanged by electrochemical reactions. After the set of CVs, the entire electrode still appears black to the eye, but the area that was inside the cell shows severe damage. The fact that the damage area has a noncircular edge on one side is attributed to trapping of bubbles against the upper edge of the cell, blocking electrochemical damage in that area. The central ∼2 mm spot containing Pd_4 has a blistered appearance, as if a thin surface layer of the GCE had delaminated from the bulk. This appearance tends to suggest that there is some gas generation below the surface of the GCE, forming bubbles that lift off the surface layer. In some areas, this thin surface layer is missing, and the exposed underlying carbon surface has a grainy, etched appearance. In either case, the damaged area appears black in the micrograph because it does not efficiently reflect the near-specular illumination.

The heavily damaged area is surrounded by an annular area that looks smooth and black to the eye but appears to have a "haze" of material on the surface that decreases specular reflectivity, leading to a dark-gray appearance. This annulus corresponds to the area of GCE that was inside the cell but outside the cluster spot. The electrodes were not rinsed after electrochemical experiments to avoid breaking off the delicate blistered structures in the central spot, and we believe that the "haze" simply corresponds to deposition of material eroded from the central spot. The dramatic nature of the electrode damage for Pt_4/GCE can be seen by comparison to the micrograph for Pt_7/GCE (Figure 5 D), which had more than 100 times longer exposure to the electrochemical environment (>10 times as many CV cycles at 10 times slower scan rate).

The obvious erosion of carbon from the CGE suggests that the gas generation observed for the Pt_4/GCE sample results from oxidation of carbon. The observation of similar, large oxidative currents for initial CVs in N_2- and O_2-saturated $HClO_4$ rules out O_2 as the oxidant. It might be thought that the perchlorate anion could be the oxidant, however, we observe (see below) similar behavior in H_2SO_4 electrolyte and thus conclude that water must be the dominant oxidant:

$$CO_2 + 4H^+ + 4e^- \leftrightarrow C + 2H_2O \qquad E^0 = 0.01\,V\ vs\ Ag/AgCl \tag{1}$$

or

$$CO + 2H^+ + 2e^- \leftrightarrow C + H_2O \qquad E^0 = 0.32\,V\ vs\ Ag/AgCl \tag{2}$$

Both reactions are thermodynamically allowed in the applied potential ranges, however, while carbon oxidation has been detected in PEMFCs at potentials >0.9 V vs NHE (∼0.7 V vs Ag/AgCl), only minor amounts of CO have been found.[30,31] We conclude, therefore, that small Pt_n clusters ($n \leq 6$) are highly efficient at catalyzing oxidation of the GCE support by water, with little overpotential. In this scenario, the current breakdown discussed above is attributed to CO_2 or CO evolution at the GCE working electrode and hydrogen evolution at the counter electrode. Note that in the experiment shown in Figure 6, roughly 1 C of charge passed the working electrode which would, according to the reaction scheme proposed above, produce ∼64 μL of CO_2 and 128 μL of H_2, compared to a cell volume of only 15 μL, consistent with the repeated current blockages from bubbles. The reaction would dissolve ∼30 μg of carbon, corresponding to removing ∼7 μm of carbon over the 2 mm diameter cluster spot.

These results are qualitatively reproducible on freshly prepared Pt_4/GCE samples, and the anomalously large currents do not depend on whether N_2- or O_2-saturated electrolyte is studied first. As noted, the immediate appearance of milliampere currents was a common feature for all Pt_n/GCE for $n \leq 6$. Every sample behaved somewhat differently (Figures S10−S16), however, this variation as well as the erratic behavior observed during CV cycling are attributed, at least in part, to variations in bubble trapping/current blockage at the electrodes.

In the reactions proposed to account for the Pt_4-catalyzed carbon oxidation, carbon is oxidized and protons are reduced, generating H_2 at the Pt counter electrode. Therefore, H_2 may diffuse to the Pt_4/GCE working electrode and be oxidized to protons, thereby contributing to the observed current. In essence, protons are reduced to H_2 at the counter electrode, transported through the solution as H_2, then reoxidized to protons at the Pt_4/GCE, with two electrons passing through the external circuit for each H_2 molecule. If we assume that the solution is at room temperature and saturated with H_2 (∼0.8 mM),[32] the peak H_2 oxidation current in the linear sweep voltammetric experiment can be computed from the following equation:[33]

$$\frac{i_p}{A} = (2.69 \times 10^5) n^{1.5} D_0^{0.5} C_0^{*} \nu^{0.5} \tag{3}$$

where i_p/A is the peak current density (A/cm^2), $n = 2$, ν is the sweep rate (1 V/s), C_0^* is the H_2 concentration (8×10^{-7} mol/cm^3), and D_0 is the H_2 diffusion coefficient (4.5×10^{-5} cm^2/s).[33] The peak current density from this mechanism is, thus, calculated to be 5 mA/cm^2. From comparison with the observed current densities, we conclude that even if the cell becomes saturated with H_2, the oxidation of H_2 cannot account for more than a few percent of the current at the Pt_4/GCE. Furthermore, because the electrolyte initially contains no dissolved H_2, this process obviously cannot be responsible for the large currents observed immediately when potential is applied to the cell. Finally, perhaps the most obvious evidence supporting carbon oxidation as the carrier for the large oxidative currents is the dramatic carbon loss observed at the Pt_4/GCE.

Electrochemistry of Pt_9 on GCEs (in Situ): A Typical Larger Cluster. Pt clusters with >7 atoms behave somewhat differently from the smaller clusters exemplified by Pt_4. Pt_8 and Pt_9 showed virtually identical electrochemical behavior, represented by the Pt_9/GCE results in Figure 7. The behavior for Pt_{10} and Pt_{11} will be discussed below. As for the small cluster samples, Pt_8 and Pt_9 show anomalously large currents, often immediately upon

dx.doi.org/10.1021/ja309868z | J. Am. Chem. Soc. 2013, 135, 3073−3086

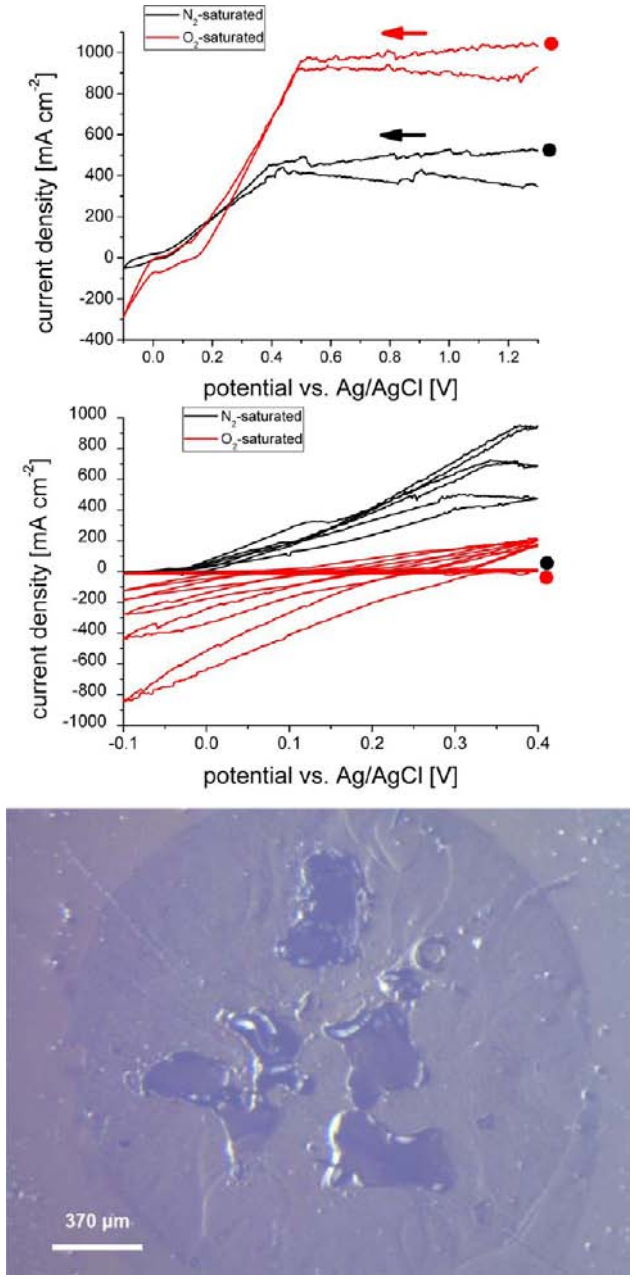

Figure 7. Pt_9/GCE *in situ* (0.1 ML Pt). (Top) CVs of Pt_9/GCE in N_2- and O_2-saturated 0.1 M $HClO_4$ at a scan rate of 10 V s^{-1} (initial scan from 1.3 to −0.1 V vs Ag/AgCl), immediate current. (Middle) CVs of Pt_9/GCE in N_2- and O_2-saturated 0.1 M $HClO_4$ at a scan rate of 1 V s^{-1}, (initial scan from 0.4 to −0.1 V vs Ag/AgCl, 100 scans), after activation. (Bottom) Optical micrograph of the Pt_9/GC electrode after the electrochemical reactions.

starting a CV (top frame for Figure 7). However, for Pt_8 and Pt_9, we also sometimes found currents that were initially in the $\mu A/cm^2$ "normal" range, quickly building to hundreds of mA/cm^2 with CV cycling (Figure 7, middle frame), as if some activation process were required to convert the clusters to a state capable of catalyzing carbon oxidation. The nature of this activation process is unclear. In experiments where large currents were observed immediately, the shape of the resulting CV was quite similar to that for Pt_4, the main difference being that the current in O_2-saturated solution is three times higher than for Pt_4. After cycling (even at 1 V s^{-1}) under conditions of high current, the cell current eventually abruptly and irreversibly goes to zero and can be restored only by breaking the seal to the GCE, so that bubbles can be flushed out with fresh electrolyte.

The bottom frame of Figure 7 shows the optical micrograph of the GCE after it was subjected to ∼250 CV cycles. As in every case where milliamp currents were observed, the glassy carbon substrate is badly damaged, with a blistered and etched appearance over the area where the clusters were deposited.

To examine the role of the perchlorate anion in the apparent oxidation of the GCE, the same experiment was also performed with 0.1 M H_2SO_4 replacing the perchloric acid but otherwise under identical conditions. The resulting CV is shown in Figure S17. As for the measurements in perchlorate solutions, milliamp currents are observed in a series of CV cycles. In this set of CVs, there is an episode where the current drops to zero but then spontaneously recovers (∼0.04 V wide excursion near 0.15 V). We attribute this type of behavior, as well as smaller current dips observed in many of the CVs, to bubbles completely or partially blocking one of the electrodes but then spontaneously clearing again. At the end of this particular set of CVs, the current dropped irreversibly to zero (transition just above 0.3 V). An optical micrograph of the GCE after reaction is given in Figure S17 as well. As in every case where large currents were observed, the surface of the glassy carbon appears etched and blistered. In this micrograph, it is particularly obvious that the heavy damage occurs only in the 2 mm cluster containing spot, which in this experiment was evidently slightly off center with respect to the cell. The glassy carbon in the region surrounding the cluster spot but still inside the cell, although somewhat discolored by contact with electrolyte, does not look markedly different than the region which was outside the cell.

Pt_{10} and Pt_{11}: Intermediate Cases. These two clusters showed behavior intermediate between Pd_7, for which large currents attributed to carbon oxidation were never observed in the >800 CVs scanned over various ranges for several independent samples, and Pt_4 or Pt_9, where the samples did catalyze carbon oxidation either immediately or after a short induction period. Pt_{10} and Pt_{11} both did show carbon oxidation in at least one CV, but in most CVs, the currents were in the "normal" range and with structure expected for Pt under these conditions.

For Pt_{11}, we only observed currents above a few mA/cm^2 in a single CV. Apart from that single CV, which terminated almost immediately because of bubble blockage, Pt_{11} showed no evidence of carbon oxidation. The top frame of Figure 8 shows a set of CVs over the full potential range in N_2-saturated solution showing peaks tentatively attributed to Pt redox and hydride adsorption/desorption. The structure is similar to that seen for Pt_{poly}, with the exception that the currents decay rapidly with cycling, presumably because this experiment runs into the potential range where Pt is oxidized, and as above, we conclude that repeated Pt oxidation/reduction leads to sintering or dissolution. The second frame compares CVs over a narrower range for O_2- and N_2-saturated solution, showing evidence for O_2 reduction, decaying with CV cycling. Finally, the micrograph taken of the Pt_{11}/GCE after CV cycling shows essentially no signs of damage.

The results for Pt_{10} are shown in the Figure S16. In essence, for some experiments large currents were observed, but in others, only currents in the $\mu A/cm^2$ range were seen in both N_2- and O_2-saturated $HClO_4$. Even the large currents seen

dx.doi.org/10.1021/ja309868z | J. Am. Chem. Soc. 2013, 135, 3073−3086

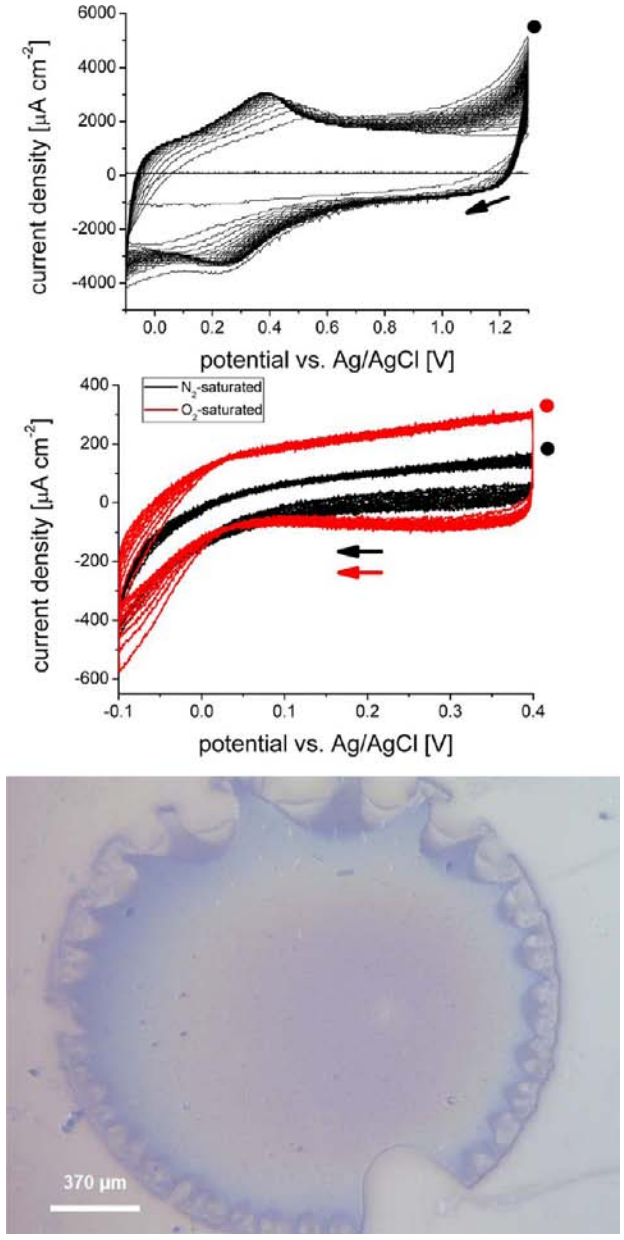

Figure 8. Pt_{11}/GCE *in situ* (0.1 ML Pt). (Top) CVs of Pt_{11}/GCE in N_2-saturated 0.1 M $HClO_4$ at a scan rate of 1 V s^{-1}, (initial scan from 1.3 to −0.1 V vs Ag/AgCl, 100 scans). The enclosed area decreases in subsequent scans indicating a loss in active Pt surface area. (Middle) CVs of Pt_{11}/GCE in N_2- and O_2-saturated 0.1 M $HClO_4$ at a scan rate of 0.1 V s^{-1} (initial scan from 0.4 to −0.1 V vs Ag/AgCl, 10 scans). (Bottom) Optical micrograph of the Pt_{11}/GC electrode after the electrochemical reactions.

occasionally were an order of magnitude smaller than those observed for Pt_4 or Pt_9. The micrograph taken after Pt_{10}/GCE was exposed to ∼200 CVs shows some signs of a blistered appearance but not the dramatic damage shown by electrodes with Pt_n (n = 1 to 6, 8, 9). Those electrodes also showed a blistered appearance near the edges of the exposed area, but over much of the area the blisters had ruptured or dissolved away, exposing strongly etched carbon underneath.

Effects of Air Exposure on the Activity of Small Pt_n. A major conclusion from the results described above is that small Pt_n deposited and studied *in situ* are highly active electrocatalysts for oxidation by water of the glassy carbon electrodes. One obvious difference in our experimental protocol, compared to conventional methods, is that our electrodes were prepared in UHV, and electrochemistry was carried out without prior exposure of the electrodes to laboratory air. In previous studies of electrochemistry on size-selected clusters deposited in vacuum by Arenz and co-workers,[9] where "normal" electrochemical currents were observed, the protocol included air exposure prior to electrochemistry. Our own reference experiments performed with polycrystalline Pt foil and with Pt-free GCEs were done after preparation in UHV, without air exposure, and those results show no sign of unusual activity, thus the results suggest that the high activity requires both small clusters and absence of air exposure. To test this hypothesis, we carried out experiments where the electrodes were exposed to air after cluster deposition, prior to electrochemistry.

To eliminate any differences that might be attributable to operating conditions, the air exposure experiments were done by removing the electrochemistry antechamber and attaching a different chamber to the UHV system to serve as a load-lock for sample exchange. The antechamber, containing the *in situ* cell and associated mounting hardware, was then set up on the benchtop, open to the atmosphere. Pt_n/GCE samples were prepared exactly as in the *in situ* work described above, then the samples were removed from the UHV system and inserted into the antechamber so that electrochemistry could be studied under identical conditions, with the exception that the samples and cell were exposed to the laboratory air for ∼30 min prior to electrochemical measurements.

First consider Pt_7 on GCE, which showed normal oxygen reduction currents in the microamp range during *in situ* CVs, with no evidence of carbon oxidation or electrode degradation (Figure 5). Analogous results for Pt_7/GCE exposed to air prior to electrochemistry are shown in the top frame of Figure 9. In contrast to the *in situ* work where waves were seen for ORR, Pt oxidation/reduction, and hydride adsorption/desorption, the air-exposed sample shows little difference between the O_2- and N_2-saturated cases, with no obvious sign of any ORR or Pt redox waves. Instead, the air-exposed sample shows pairs of reduction and oxidation peaks at ∼0.22 and ∼0.87 V vs Ag/AgCl, with amplitudes of a few hundred $\mu A/cm^2$ for both N_2- and O_2-saturated conditions. The origin of these symmetric reduction/oxidation features is tentatively attributed to reversible reduction/oxidation of some adventitious organic species adsorbed to the Pt_7 during air exposure. This behavior persists throughout more than 200 CV cycles in N_2-saturated $HClO_4$ and more than 500 cycles in O_2-saturated solution, even though the CVs go into the range where Pt oxidation/reduction is expected. Evidently, the adsorbates bind strongly to small Pt clusters, making cleaning by electrochemical cycling difficult. It is possible that even more aggressive electrochemical cleaning might remove the adsorbates, however, it would also most likely remove the Pt clusters, as suggested by the results in Figure 5C. There was no evidence of bubble formation in any of the CVs, and examination of the electrode after ∼1000 CV cycles showed no evidence of degradation.

The behavior of the air-exposed samples varied somewhat. Consider Pt_4 and Pt_9: In absence of air exposure, these samples showed electrochemical currents in the hundreds of mA/cm^2 range and dramatic etching of the GCEs, attributed to Pt-catalyzed carbon oxidation by water. There may have also been oxygen reduction and Pt oxidation/reduction, but these would not have been observable due to the overwhelming carbon

dx.doi.org/10.1021/ja309868z | *J. Am. Chem. Soc.* 2013, 135, 3073−3086

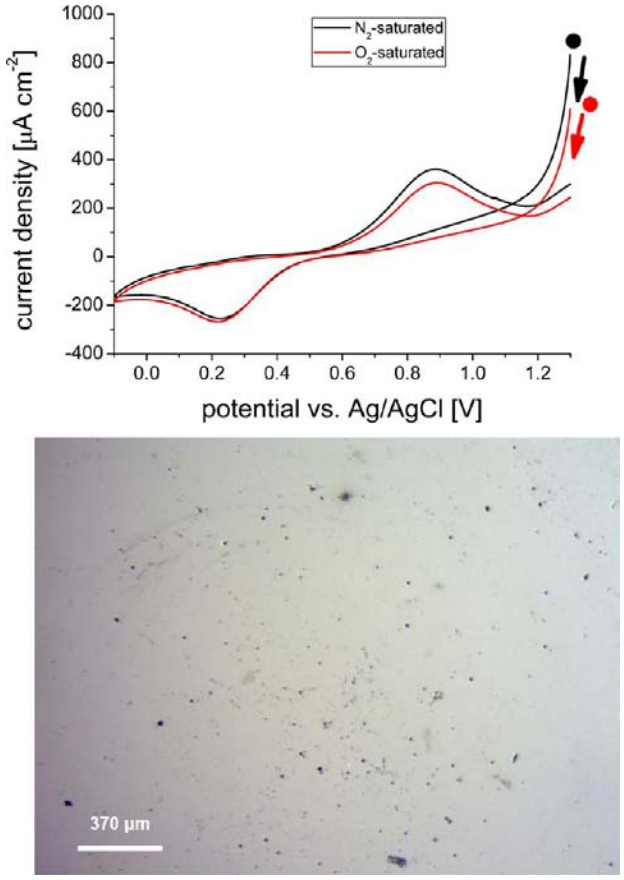

Figure 9. Pt_7/GCE *ex situ* (0.1 ML Pt). (Top) CVs of Pt_7/GCE in N_2- and O_2-saturated 0.1 M $HClO_4$ at a scan rate of 0.1 V s^{-1} (initial scan from 1.3 to −0.1 V vs Ag/AgCl). (Bottom) Optical micrograph of the Pt_7/GC electrode after the electrochemical reactions, shown is a region within the perimeter of the electrochemical cell.

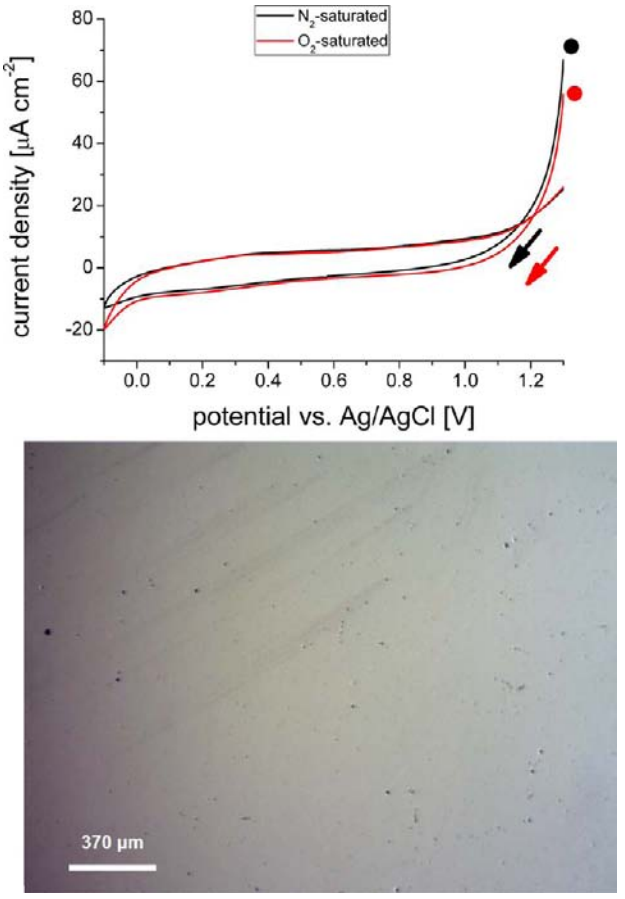

Figure 10. Pt_4/GCE *ex situ* (0.1 ML Pt). (Top) CVs of Pt_4/GCE in N_2- and O_2-saturated 0.1 M $HClO_4$ at a scan rate of 0.1 V s^{-1} (initial scan from 1.3 to −0.1 V vs Ag/AgCl). (Bottom) Optical micrograph of the Pt_4/GCE electrode after the electrochemical reactions.

oxidation current. As shown in the top frames of Figure 10 for Pt_4/GCE and Figure 11 for Pt_9/GCE, air exposure prior to electrochemistry completely suppresses the oxidation of the GCE and the milliamp currents. Instead, for both N_2- and O_2-saturated 0.1 M $HClO_4$, only 20−40 $\mu A/cm^2$ currents are observed, with little obvious structure. The magnitudes of the currents are similar to those observed for Pt-free glassy carbon electrodes, as shown in Figure 2. Evidently, for these clusters, which are highly active *in situ*, air exposure almost completely passivates the Pt, such that neither oxygen reduction nor carbon oxidation is efficient, and even oxidation and reduction of the Pt itself is suppressed. The CVs show no suggestion of bubble formation nor do the micrographs (Figures 10 bottom and 11 middle frames) taken after the series of >100 CVs, show any evidence of electrode degradation, consistent with inertness of the deposited Pt clusters. Results for *ex situ* electrochemistry studies of Pt_3/GCE, Pt_5/GCE, and Pt_6/GCE are shown in Figures S18, S19, and S20.

From comparison of all the *ex situ* results, it appears that there might be some variation in the extent of passivation with cluster size, however, it is important to recognize that the atmosphere in our building is not well controlled, and therefore it is not unreasonable to expect that the composition of organic molecules present is variable. Different organic species would tend to have different redox behavior and might result in different types of Pt passivation behavior, thus it is not unlikely that the differences partly or entirely reflect changes in the atmosphere, rather than cluster size effects.

The bottom frame of Figure 11 shows a different type of air exposure experiment. As already discussed, and shown in Figure S17, Pt_9/GCE was studied *in situ* (without air exposure) in 0.1 M H_2SO_4 solution, to help resolve the question of whether the perchlorate anion is involved in the large oxidative currents. After completing the *in situ* sulfuric acid CV experiment shown in Figure S17, the cell−electrode seal was broken, and at the same time, the antechamber was opened. In this way, the Pt_9 sample, which had catalyzed efficient carbon oxidation *in situ*, was exposed to laboratory air. After 30 min of air exposure, the cell was again sealed to the Pt_9/GCE sample and filled with N_2-saturated H_2SO_4, to see if air exposure in the middle of a set of CV experiments would suppress carbon oxidation (Figure 11, bottom frame). When CV cycling was first started after air exposure, the current was small (undetectable for the potentiostat range used), suggesting that there was an air-exposure passivation effect. With CV cycling, however, the current rapidly grew into the hundreds of mA/cm^2 range. It is important to note that in this experiment, the sulfuric acid electrolyte was not rinsed from the surface nor was the electrode deliberately dried during the air exposure. It is not unlikely, therefore, that a layer of sulfuric acid remained on the electrode surface, partially protecting it from the effects of air exposure.

dx.doi.org/10.1021/ja309868z | *J. Am. Chem. Soc.* 2013, 135, 3073−3086

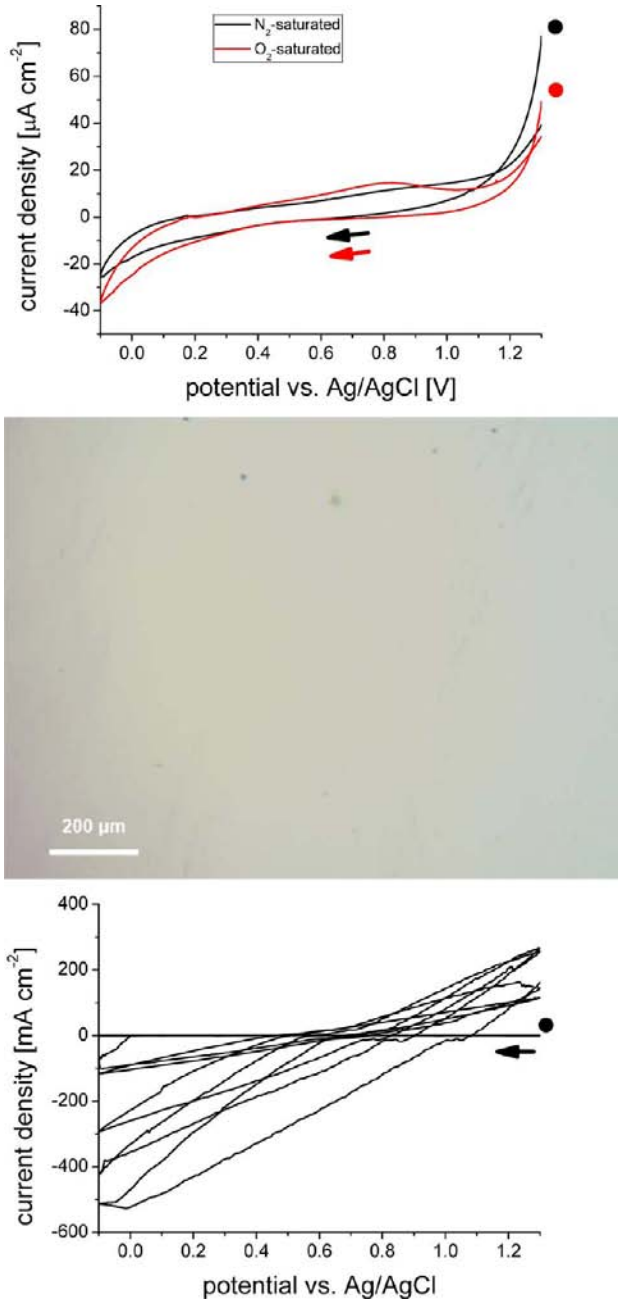

Figure 11. Pt_9/GCE *ex situ* (0.1 ML Pt). (Top) CVs of Pt_9/GCE in N_2- and O_2-saturated 0.1 M $HClO_4$ at a scan rate of 0.1 V s^{-1} (initial scan from 1.3 to −0.1 V vs Ag/AgCl). (Middle) Optical micrograph of the Pt_9/GCE electrode after the electrochemical measurements. (Bottom) CVs of Pt_9/GCE in N_2-saturated 0.1 M H_2SO_4 after *in situ* electrochemistry in H_2SO_4 (see Figure S17) and 30 min of exposure to air in the same arrangement, 100 cycles at a scan rate of 1 V s^{-1} (initial scan from 1.3 to −0.1 V vs Ag/AgCl).

■ DISCUSSION

Previously, even the smallest Pt clusters prepared by chemical and physiochemical means showed electrochemical behavior which qualitatively resembles that of polycrystalline bulk Pt,[6−9] i.e., there is a difference in the CV response between N_2- and O_2-saturated solution, and the results in N_2-saturated solution show faradaic currents due only to Pt oxidation and hydrogen adsorption. The smallest Pt clusters that were previously synthesized via a wet chemical procedure are Pt_{12} clusters stabilized in a dendrimer template, and they show a mass activity toward oxygen reduction 12 times higher than commercial catalysts.[8] Kunz et al. have prepared Pt_{20} and Pt_{46} in vacuum with a laser ablation source and mass selection by a quadrupole bender and tested their oxygen reduction activity *after air exposure*, finding the usual ORR behavior.[9] In our experiments, we find that mass-selected Pt_1−Pt_{11} studied on GCEs without air exposure show, with a few exceptions, currents attributed to electrocatalysis of carbon oxidation by water (eqs 1 and 2), resulting in currents that are 3 orders of magnitude larger than those expected for ORR. These large currents are suppressed by brief exposure to laboratory air.

Carbon oxidation has been observed in proton exchange membrane fuel cells but only at potentials >0.7 V vs Ag/AgCl.[30,31] It appears that for very small Pt_n, without air exposure, the reaction can occur with almost no overpotential. A possible catalytic cycle might involve oxidation of small Pt clusters, forming Pt oxides that then oxidize the glassy carbon support (taking CO_2 production for example):

$$Pt_n + H_2O \rightarrow Pt_nO_x \quad \text{(oxygen activation)} \tag{4}$$

$$Pt_nO_x + C \rightarrow CO_2 + Pt_n \quad \text{(carbon oxidation)} \tag{5}$$

$$C + 2H_2O \rightarrow CO_2 + H_2 \quad \text{(net)} \tag{6}$$

The high efficiency of the reaction for small Pt clusters may reflect some combination of easier oxidation of small clusters compared to bulk Pt and Pt nanoparticles (due to lower Pt−Pt coordination) or less stable nanoscale oxide (Pt_nO_x), making transfer of O to the carbon support more facile. It is worth noting that the oxidation potentials of small clusters, e.g., silver, tend to shift toward negative values when going to smaller clusters.[34]

The almost complete suppression of carbon oxidation, ORR, and Pt redox chemistry by exposure of Pt_n/GCE to air suggests that adventitious adsorbates bind strongly to the clusters, passivating the surface or converting the Pt to an inactive form. We were unable to reactivate the Pt_n/GCE samples by electrochemical cycling, however, we did not attempt cycling into potential ranges where water electrolysis might help clear the surface, for fear that this would also simply dissolve the small Pt clusters.

The remaining question is why certain size Pt_n are completely (Pt_7) or largely (Pt_{10}, Pt_{11}) inactive for carbon oxidation *in situ*. Consider Pt_7/GCE, which showed no sign of carbon oxidation but "normal" ORR and Pt redox and hydride adsorption/desorption chemistry. The literature on mass-selected Pt clusters does not reveal anything special about Pt_7. For example, in mass spectra of Pt_n^+, there is no sign that Pt_7 might be a particularly stable "magic" number cluster,[35−37] and both experimental and theoretical ionization potentials and electron affinities also do not suggest anything special about Pt_7.[38−42] Platinum clusters have been used as catalysts in the gas phase, on MgO or TiO_2 in several reactions like the dehydrogenation of hydrocarbons,[33] methane activation,[34,43,44] or CO oxidation,[45−48] with no unusual properties of Pt_7. Even studies of CO adsorption on $Pt_n^{+/0/-}$ in the gas phase show the expected behavior for Pt_7 clusters.[49]

Of course, the important question is what special properties Pt_7 (and Pt_{10}, Pt_{11}) might have when deposited on glassy carbon, because interaction with the support clearly may significantly modify both electronic and chemical properties. The one obvious sign of special properties for Pt_7/GCE, Pt_{10}/

dx.doi.org/10.1021/ja309868z | J. Am. Chem. Soc. 2013, 135, 3073−3086

GCE, and Pt_{11}/GCE is the fact that these three samples all have anomalously high Pt $4f_{7/2}$ core level binding energies, when compared to neighboring clusters (Figure 4). This pattern suggests that high core level binding energy may be correlated with low activity for catalysis of oxidation reactions. In this context, it is interesting to note that for $Pd/TiO_2(110)$, a similar size-dependent correlation was observed between high Pd core level (Pd 3d) binding energies and low activity for CO oxidation under UHV conditions.[50] The interesting question is why core levels, which are not directly involved in chemistry, should be strongly correlated with activity.

Core level binding energies are the energy difference between the initial state of the system and the photoemission final state, which consists of a cluster with a core hole on one of the atoms. In bulk Pt, conduction electrons can flow to screen the core hole, stabilizing the final state. In a small cluster on an insulating surface, there is a final state charging energy associated with localizing the charge, which is inversely proportional to cluster radius in the limit of isolated spherical clusters. In addition, core hole screening in very small clusters is limited to polarization of the valence orbitals, because there are no delocalized conduction electrons. Both effects tend to result in small clusters having significantly higher core level binding energies than bulk metal and a general trend toward decreasing binding energy with increasing size.[51−53] For clusters on a conductive support, screening by support electrons may moderate this trend to some extent; nonetheless, the data in Figure 4 clearly show that there is a general trend of decreasing Pt 4f binding energy with increasing size.

The size-dependent fluctuations in binding energy appear to be correlated with catalytic activity. There are two effects to consider. If a particular cluster has a tendency to accept or donate electron density in binding to the support, then this partial charging of the cluster can result in "chemical" or initial state shifts in the binding energy, because electrons are more strongly bound to positively charged centers and vice versa. In addition, if a cluster has closed shell or otherwise particularly stable valence electronic structure, then the valence shell may be less able to polarize in order to screen the final state core hole, also leading to a shift to higher binding energy. For Pt_7/GCE, it is not clear which of these effects is most responsible for the fluctuations in Pt 4f binding energy, however, this is a question that should be quite amenable to theoretical investigation.

CONCLUSIONS

Investigating the smallest possible Pt structures in the form of size-selected Pt_n clusters from a laser ablation source deposited on GCEs for their oxygen reduction activity reveals several interesting electrocatalytic effects. The most notable finding is that many of the small Pt particles studied *in situ*, with no air exposure, efficiently catalyze the oxidation of carbon by water, resulting in current densities approaching 1 A/cm^2. Due to their unusually high activity for carbon oxidation, the active Pt_n might also be interesting catalysts for reactions like the decomposition of methanol/ethanol at the anode of a direct methanol/ethanol fuel cell, because current electrocatalysts for the decomposition of carbon-containing compounds lead to sluggish reaction and C−C bonds are generally not broken.[2]

The tendency of the small Pt_n to catalyze carbon oxidation is highly variable and appears to be correlated with the Pt 4f core level binding energy. Systems with relatively low binding energy are all highly active, while Pt_7, Pt_{10}, and Pt_{11}, which are local maxima in the trend of Pt 4f binding energy with size, are all relatively inactive. We speculate that this correlation results from the fact that Pt clusters which have particularly stable valence electrons should tend to be relatively inactive, and these stable, low polarizability valence shells should also tend to be ineffective at screening the photoemission final state, resulting in high binding energy.

Finally, we find that air exposure prior to electrochemistry has a huge passivating effect on the activity of the small Pt_n. One might think that this sensitivity renders these catalysts useless from any practical perspective, however, we note that the catalysts appear to be protected from air passivation simply by coating them with electrolyte prior to air exposure, thus it should be possible to prevent the passivation on practical time scales.

The result that there is dramatic size-dependent variation in carbon oxidation activity for small Pt clusters, apparently correlated with the Pt 4f binding energy, is quite interesting from a fundamental perspective, but there may be practical implications as well. The carbon oxidation reaction is coupled with H_2 generation at the counter electrode, and this might serve as a compact H_2 source with net energy cost of ∼40 kJ per mole hydrogen, which is substantially better than that for H_2 from water electrolysis, for example (∼240 kJ per mole hydrogen). The net reaction as studied here (with $2H^+ + 2e^- \rightarrow H_2$ as the reduction half-cell) is endoergic, however, with an appropriate reduction half-cell, carbon oxidation could be a compact electric energy source as well. Finally, carbon electrode corrosion is a significant problem in carbon-supported electrocatalysis.[31,54−56] The fact that we see dramatic carbon oxidation with most of the small Pt_n but see no carbon oxidation for Pt_{nano} under similar conditions (and with 10 times the Pt loading), suggests that perhaps small Pt clusters are particularly destructive in this regard. If confirmed in further work, then this result would suggest that there is a trade-off involved in increasing the dispersion of Pt on carbon electrodes. The mass activity may increase, but this increase may come at the cost of increased electrode corrosion.

ASSOCIATED CONTENT

Supporting Information

Additional figures clarifying and confirming the present work are presented. The material is available free of charge via the Internet at http://pubs.acs.org.

AUTHOR INFORMATION

Corresponding Author

anderson@chem.utah.edu

Notes

The authors declare no competing financial interest.

ACKNOWLEDGMENTS

This work was supported by the U.S. Department of Energy, Condensed Phase and Interfacial Molecular Science program grant no. DEFG03-99ER15003. S.P. is grateful for a research fellowship from the German Research Foundation (DFG) grant no. PR-1234 2/1.

REFERENCES

(1) Gasteiger, H. A.; Kocha, S. S.; Sompalli, B.; Wagner, F. T. *Appl. Catal., B* **2005**, *56*, 9−35.

(2) Gasteiger, H. A.; Garche, J. *Handbook of Heterogeneous Catalysis*, Wiley: Hoboken, NJ, 2008; pp 3081−3121.

(3) Gasteiger, H. A. *Science* **2009**, *324*, 48−49.
(4) Raimondi, F.; Scherer, G. G.; Kötz, R.; Wokaun, A. *Angew. Chem., Int. Ed.* **2005**, *44*, 2190−2209.
(5) Lim, B.; Jiang, M.; Camargo, P. H. C.; Cho, E. C.; Tao, J.; Lu, X.; Zhu, Y.; Xia, Y. *Science* **2009**, *324*, 1302−1305.
(6) Shao, M.; Peles, A.; Shoemaker, K. *Nano Lett.* **2011**, *11*, 3714−3719.
(7) Nesselberger, M.; Ashton, S.; Meier, J. C.; Katsounaros, I.; Mayrhofer, K. J. J.; Arenz, M. *J. Am. Chem. Soc.* **2011**, *133*, 17428−17433.
(8) Yamamoto, K.; Imaoka, T.; Chun, W.-j.; Enoki, O.; Katoh, H.; Takenaga, M.; Sonoi, A. *Nat. Chem.* **2009**, *1*, 397−402.
(9) Kunz, S.; Hartl, K.; Nesselberger, M.; Schweineberger, F. F.; Kwon, G.; Hanzlik, M.; Mayrhofer, K. J. J.; Heiz, U.; Arenz, M. *Phys. Chem. Chem. Phys.* **2010**, *12*, 10288−10291.
(10) Hartl, K.; Nesselberger, M.; Mazrhofer, K. J. J.; Kunz, S.; Schweineberger, F. F.; Kwon, G.; Hanzlik, M.; Heiz, U.; Arenz, M. *Electrochim. Acta* **2010**, *56*, 810−816.
(11) Van der Linden, W. E.; Dieker, J. W. *Anal. Chim. Acta* **1980**, *119*, 1−24.
(12) Schulenburg, H.; Müller, E.; Khelashvili, G.; Roser, T.; Bönnemann, H.; Wokaun, A.; Scherer, G. G. *J. Phys. Chem. C* **2009**, *113*, 4069−4077.
(13) Jenkins, G. M.; Kawamura, K. *Nature* **1971**, *231*, 175−176.
(14) Jenkins, G. M.; Kawamura, K.; Ban, L. L. *Proc. R. Soc. London, Ser. A* **1972**, *327*, 501−517.
(15) Harris, P. J. F. *Philos. Mag.* **2004**, *84*, 3159−3167.
(16) Heiz, U.; Vanolli, F.; Trento, L.; Schneider, W. D. *Rev. Sci. Instrum.* **1997**, *68*, 1986−1994.
(17) Boyd, K. J.; Lapicki, A.; Aizawa, M.; Anderson, S. L. *Rev. Sci. Instrum.* **1998**, *12*, 4106−41015.
(18) Boyd, K. J.; Lapicki, A.; Aizawa, M.; Anderson, S. L. *Nucl. Instrum. Methods Phys. Res., Sect. B* **1999**, *157*, 144−154.
(19) Lapicki, A.; Boyd, K. J.; Anderson, S. L. *J. Vac. Sci. Technol., A* **2000**, *18*, 2603−2605.
(20) Aizawa, M.; Lee, S.; Anderson, S. L. *J. Chem. Phys.* **2002**, *117*, 5001−5011.
(21) Paulus, U. A.; Wokaun, A.; Scherer, G. G.; Schmidt, T. J.; Stamenkovic, V.; Markovic, N. M.; Ross, P. N. *Electrochim. Acta* **2002**, *47*, 3787−3798.
(22) Savinova, D. V.; Molodkina, E. B.; Danilov, A. I.; Polukarov, Y. M. *Russ. J. Electrochem.* **2004**, *40*, 683−687.
(23) Srejic, I.; Smiljanic, M.; Rakocevic, Z.; Strbac, S. *Int. J. Electrochem. Sci.* **2011**, *6*, 3344−3354.
(24) Barr, T. L. *J. Vac. Sci. Technol., A* **1989**, *7*, 1677−1683.
(25) Watanabe, Y.; Wu, X.; Hirata, H.; Isomura, N. *Catal. Sci. Technol.* **2011**, *1*, 1490−1495.
(26) Dulub, O.; Hebenstreit, W.; Diebold, U. *Phys. Rev. Lett.* **2000**, *84*, 3646−3649.
(27) Hubbell, J. H.; Seltzer, S. M. Tables of X-ray mass attenuation coefficients and mass energy-absorption coefficients from 1 keV to 20 MeV for elements z = 1−92 and 48 additional substances of dosimetric interest. *NISTIR 5632*; Physical Measurement Laboratory, NIST: Gaithersburg, MD.
(28) Powell, C. J.; Jablonski, A. *NIST electron effective-attenuation-length database*, 1.0 ed.; NIST: Gaithersburg, MD, 2001.
(29) Ferreira, P. J.; la O', G. J.; Shao-Horn, Y.; Morgan, D.; Makharia, R.; Kocha, S. S.; Gasteiger, H. A. *J. Electrochem. Soc.* **2005**, *152*, A2256−A2271.
(30) Avasarala, B.; Moore, R.; Haldar, P. *Electrochim. Acta* **2010**, *55*, 4765−4771.
(31) Borup, R.; Meyers, J.; Pivovar, B.; Kim, Y. S.; Mukundan, R.; Garland, N.; Meyers, D.; Wilson, M.; Garzon, F.; Wood, D.; Zelenay, P.; More, K.; Stroh, K.; Zawodzinski, T.; Boncella, J.; McGrath, J. E.; Inaba, M.; Miyatake, K.; Hori, M.; Ota, K.; Ogumi, Z.; Miyata, S.; Nishikata, A.; Siroma, Z.; Uchimoto, Y.; Yasuda, K.; Kimijima, K.-I.; Iwashita, N. *Chem. Rev.* **2007**, *107*, 3904−3951.
(32) Linke, W. F. *Solubilities of Inorganic and Metal-Organic Compounds*, 4th ed., , Van Nostrand: Princeton, N. J., 1958; Vol. *1*, pp 1075−83.
(33) Ferrell, R. T.; Himmelblau, D. M. *AIChE J.* **1967**, *13*, 702−708.
(34) Bard, A. J.; Faulkner, L. R. *Electrochemical Methods: Fundamentals and Applications*, Wiley: Hoboken, NJ, 2001.
(35) Trevor, D. J.; Whetten, R. L.; Cox, D. M.; Kaldor, A. *J. Am. Chem. Soc.* **1985**, *107*, 519−520.
(36) Trevor, D. J.; Cox, D. M.; Kaldor, A. *J. Am. Chem. Soc.* **1990**, *112*, 3742−3749.
(37) Fayet, P.; Patthey, F.; Roy, H.-V.; Detzel, T.; Schneider, W.-D. *Surf. Sci.* **1992**, *269*, 1101−1108.
(38) Ervin, K. M.; Ho, J.; Lineberger, W. C. *J. Chem. Phys.* **1988**, *89*, 4514−4521.
(39) Taylor, S.; Lemire, G. W.; Hamrick, Y. M.; Fu, Z.; Morse, M. D. *J. Chem. Phys.* **1988**, *89*, 5517−5523.
(40) Ho, J.; Polak, M. L.; Ervin, K. M.; Lineberger, W. C. *J. Chem. Phys.* **1993**, *99*, 8542−8551.
(41) Pontius, N.; Bechthold, P. S.; Neeb, M.; Eberhardt, W. *J. Electron Spectrosc. Relat. Phenom.* **2000**, *106*, 107−116.
(42) Nie, A.; Wu, J.; Zhou, C.; Yao, S.; Luo, C.; Forrey, R. C.; Cheng, H. *Int. J. Quantum Chem.* **2007**, *107*, 219−224.
(43) C. Adlhart, C.; E. Uggerud, E. *Chem. Commun.* **2006**, 2581−2582.
(44) Harding, D. J.; Kerpal, C.; Meijer, G.; Fielicke, A. *Angew. Chem., Int. Ed.* **2012**, *51*, 817−819.
(45) Shi, Y.; Ervin, K. M. *J. Chem. Phys.* **1998**, *5*, 1757−1760.
(46) Balaj, O. P.; Balteanu, I.; Roßteuscher, T. T. J.; Beyer, M. K.; Bondybey, V. E. *Chem. Phys.* **2004**, *43*, 6519−6522.
(47) Balteanu, I.; Balaj, O. P.; Beyer, M. K.; Bondybey, V. E. *Phys. Chem. Chem. Phys.* **2004**, *6*, 2910−2913.
(48) Y. Watanabe, Y.; I. Noritake, I. *J. Sci. Vac. Technol., A* **2009**, *27*, 1153−1158.
(49) Gruene, P.; Fielicke, A.; Meijer, G.; Rayner, D. M. *Phys. Chem. Chem. Phys.* **2008**, *10*, 6144−6149.
(50) Kaden, W. E.; Wu, T.; Kunkel, W. A.; Anderson, S. L. *Science* **2009**, *326*, 826−829.
(51) Kuhrt, C.; Harsdorff, M. *Surf. Sci.* **1991**, *245*, 173−179.
(52) Wertheim, G. K.; DiCenzo, S. B. *Phys. Rev. B* **1988**, *37*, 844−847.
(53) Chusuei, C. C.; Lai, X.; Luo, K.; Goodman, D. W. *Top. Catal.* **2001**, *14*, 71−83.
(54) Zhang, S.; Yuan, X.-Z.; Hin, J. N. C.; Wang, H.; Friedrich, K. A.; Schulze, M. *J. Power Sources* **2009**, *194*, 588−600.
(55) Madden, T.; Perry, M.; Protsailo, L.; Gummalla, M.; Burlatsky, S.; Cipollini, N.; Motupally, S.; Jarvi, T. *Handb. Fuel Cells* **2009**, *6*, 861−879.
(56) Meier, J. C.; Galeano, C.; Katsounaros, I.; Topalov, A. A.; Kostka, A.; Schueth, F.; Mayrhofer, K. J. J. *ACS Catalysis* **2012**, *2*, 832−843.